ELSEVIER

Journal of Alloys and Compounds 229 (1995) 10–23

Journal of ALLOYS AND COMPOUNDS

Interstitially-stabilized cluster-based halides of the early transition metals

John D. Corbett

Department of Chemistry, Iowa State University, Ames, IA 50011, USA

Received 27 February 1995; in final form 3 March 1995

Abstract

A large number of reduced halides of the first two groups of transition metals are obtained that are built from edge-bridged octahedral cluster units (M_6X_{12}) but only when these contain a centered (interstitial) heteroatom Z. The third component provides not only central bonding to the M_6X_{12} cluster but also valence electrons that aid in fulfilling certain minimal electron counts necessary in clusters of these electron-poor metals. Recent results are surveyed for zirconium and the rare-earth metals (group 3 plus the lanthanides). Much of the versatility and beauty of zirconium cluster phases originate with the diverse ways for intercluster bridging by additional halide plus a choice of 15 examples of Z. Some new tunnel, perovskite derivative, and network structures, as well as bonding and electronic regularities are described for these. Rare-earth metal examples afford substantial contrasts with only a few ternary examples that contain isolated clusters, these also being hypostoichiometric with fewer than 12X per 6M. Other phases formed contain either tetrameric oligomers or infinite chains constructed from classical clusters that have been condensed through sharing of metal edges. The rare-earth element examples are noteworthy in their ability to bind 18 different Z, which include 13 of the 3d, 4d or 5d metals as the interstitial component. Some relevant properties are also described.

Keywords: Halide clusters; Transition metals; Rare-earth metals; Structures

1. Introduction

Exploratory synthesis in the search for new compounds, structures and properties is an important aspect of materials chemistry. In fact, the products of these efforts may often turn out to be unprecedented and even unimaginable; that is, "gold is still where you find it". A unique field of solid state chemistry has been discovered that is associated almost entirely with reduced halides of the first two transition-metal groups, namely for Zr, Hf (Ti, Th) and the rare-earth elements R (Sc, Y and the lanthanides La–Lu) with halides X = Cl, Br, I [1–3]. The nominally octahedral metal clusters present in all of these are evidently stable only when centered by one of a sizeable number of interstitial heteroelements Z, at least for phases prepared under equilibrium (high temperature) conditions. (Surface 'interstitials' and room temperature kinetic routes need to be included when Z = H [4,5].) The typical cluster is insulated from its environment by 12 edge-bridging halogen atoms X^i (Fig. 1) plus, as shown, additional halide atoms X^a from some source that bond to, and often bridge between, metal vertices, since these positions are evidently also strongly bonding sites. The surprising variety of modes for these interconnections will be considered shortly. With rare-earth-metal atoms, condensation of the $R_6(Z)$ clusters, nearly always by edge-sharing, is relatively common, and these products remain sheathed by halide bonded to the exposed cluster edges and vertices.

The compounds formed by zirconium (and hafnium) vs. those formed by the rare-earth elements are almost exclusive classes; zirconium nearly always forms network structures involving isolated clusters, the only exceptions apparently being the binary ZrCl, ZrBr which can be viewed as $\bar{3}$ Zr_6X_8-type (face-capped) clusters condensed around the waists into double-metal sheets. Evidently only a limited number of the zirconium cluster types may be centered by 3d transition metals. On the contrary, the rare-earth elements form only three ternary structure types with isolated clusters, and these have metal-rich stoichiometries as

SSDI 0925-8388(95)01684-8

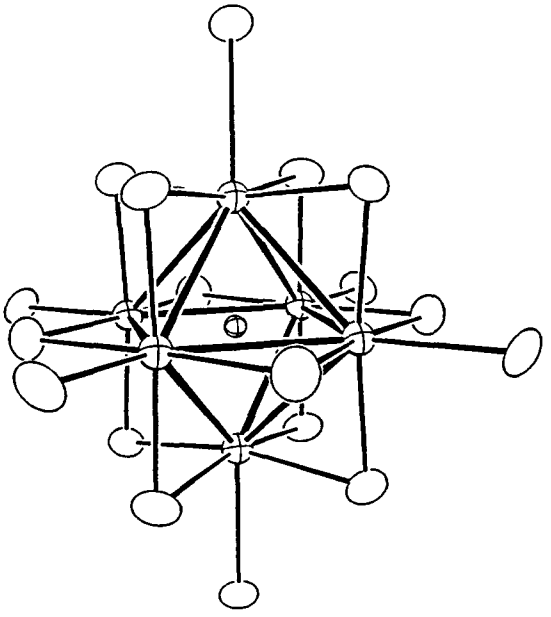

Fig. 1. An $M_6(Z)X_{12}$ cluster unit with six additional X^a halide atoms at the cluster vertices. (Zr and the centered interstitial Z are drawn with crossed ellipsoids.)

well, $R_{12}X_{17}(Z_2)$, $R_6X_{10}(Z)$ and $R_7X_{12}(Z)$. Only the last is a recognizable derivative of $Zr_6X_{12}(Z)$ members. (Although Z is systematically listed last in most formulas, it is always located within the Zr_6 or R_6 framework.) All the other reduced R products are condensed chain examples, nine types in all. (Layered ternary products exist too but will not be considered.) A pleasant surprise on the way to chains is the occurrence of an appreciable number of stable intermediate oligomers in which four clusters are condensed in a 2 + 2 manner. All three types of these R products are obtainable with a variety of later 3d, 4d and 5d elements as interstitials.

The coverage of these compounds will be selective, largely featuring recent results from the author's laboratories. The zirconium cluster principles and many examples were described fairly thoroughly both in 1989 [1] and in a 1992 overview of mainly the crystallographic and structural aspects [3]. Recent results with 3d interstitials, $Zr_6X_{15}(Z)$ networks, double salts $A_xMCl_6 \cdot Zr_6(Z)Cl_{12}$, and some novel tunnel structures will be noted here. Rare-earth-metal halide systems in oxidation states below two were covered in a thorough fashion in a review of the literature through 1988 plus some from 1989 by Simon et al. [2]. Notice of nearly all of the halide phases with transition metal interstitials in chains as well as the R-rich cluster and oligomer phases has appeared since then. However, five older chain structure types known only with carbon or neighboring B, N interstitials and scandium (Sc_5Cl_8C, Sc_4Cl_6B, $Sc_7Cl_{10}C_2$) or yttrium ($Y_6I_7C_2$ and $Y_{10}I_{13}C_2$) will not be considered further. The same exclusion applies to diverse structures that are evidently unique for dicarbon in clusters, dimers and chains, the cluster units in all being elongated to accommodate this group. It should also be noted that there are indeed a few truly binary and metal–metal bonded halide phases for these two types of elements: (a) the double-metal-layered ZrCl and ZrBr (the only condensed Zr examples) which also have a modest interstitial chemistry; (b) the original discovery in this area, Gd_2Cl_3, and a few relatives that are constructed of face-capped (M_6X_8) clusters condensed via edge sharing; (c) the empty Sc_7Cl_{10}, a close relative of the above carbide; and (d) the recently discovered NiAs-type LaI [6]. The first three types appear mainly in the older literature. A sizeable variety of double-metal-layered R_2X_2Z and R_2XZ types also exist, but only as ternary compounds with Z = H, C, N, Fe, etc., and many of these have been reviewed as well [2]. The interstitials that were unknowingly present in the earliest investigations of many cluster phases were adventitious in nature and caused considerable confusion and not a few errors regarding pseudo-binary phases that were really ternary, but substantially all of these problems have now been cleared up.

Clustering is a common property of transition metal systems when (a) the proportion of nonmetal atoms is reduced well below the preferred coordination number of the metal, six for example, (b) the transition metals occur fairly early in their periods so that the d orbitals are relatively large, and (c) some valence electrons remain for metal–metal bonding. This is a common situation for niobium and tantalum cluster systems [7,8]. The interstitials come into play with earlier and electron-poorer host metals in supplementing the filling of a certain minimum number of cluster-bonding orbitals. They of course contribute central bonding as well.

2. Zirconium cluster systems

With virtually no exceptions, the great variety of zirconium cluster halides fit into the general composition description $A_x^i[Zr_6(Z)X_{12}^i]X_n^a$ where $0 \leq n \leq 6$ additional halides are bonded at vertex sites on the centered 6–12 cores, Fig. 1. This generates a bridged network except for $n = 6$ (e.g. $Zr_6(Z)X_{12}X_6$). In addition, x alkali-metal cations (occasionally alkaline-earth elements) may be accommodated within halogen-bounded cavities, presently over the range $0 \leq x \leq 6$. The electronic bases for the need of cations, which is driven by the choice of Z and the magnitude of n, will be described later.

The considerable structural variety derives in good part from the evident requirement that halogen atoms (or other ligands) be bound exo (X^a) at all six cluster vertices. The modes whereby this commonly occurs

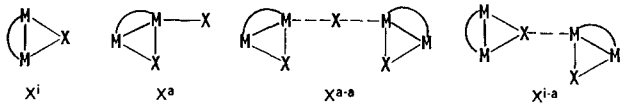

1

are shown in **1** where M–M represents an edge of the metal cluster, the first example shown bonding only X^i. At one limit ($n = 0$), half of the inner edge-bridging X^i are forced to double up as X^{i-a}, that is, to be three-coordinate, bonding over one edge and to a (more distant) vertex in another cluster. The way this is accomplished in $Zr_6(Z)X_{12}$ members, Z = H, Be, B or C, is shown in a [110] projection in Fig. 2, which will be clearer in its three-dimensional import when it is realized that a vertical 3-fold axis runs through each centered Z and these lie on an inversion center. A useful abbreviation of the connectivity is $Zr_6(Z)X^i_6X^{i-a}_6$ or, if the common sum of 12 edge-bridging and 6 exo functions is to be evident, as the more elaborate $Zr_6(Z)X^i_6(X^{i-a})_{6/2}(X^{a-i})_{6/2}$. (A different version of this rhombohedral network that allows a large cation to be accommodated [9] is also known.) Progression through compounds with higher n values in principle occurs structurally with the successive conversion of the halide functions from X^{i-a} to X^{a-a}, extra halide that is bridging only between vertices, and then to X^a, which is exo at only one vertex. Each of these three is represented in **1** (right to left respectively). This trend is for the most part as observed, the outer halide modes progressing regularly through what is also an order of increasing basicity ($i-a < a-a < a$). However, other factors may intercede. The first example discovered for a 6–13 proportion was an exception, $Zr_6Cl_{13}B$ [1], namely $Zr_6(B)(Cl^i)_{10}(Cl^{i-i})_{2/2}(Cl^{a-a-a})_{6/3}$ with two new types of halide functionality, one that is simultaneously edge-bridging in two clusters ($i-i$) and an exo atom that only bonds to three vertices. Fig. 3 shows a recent higher symmetry example found for

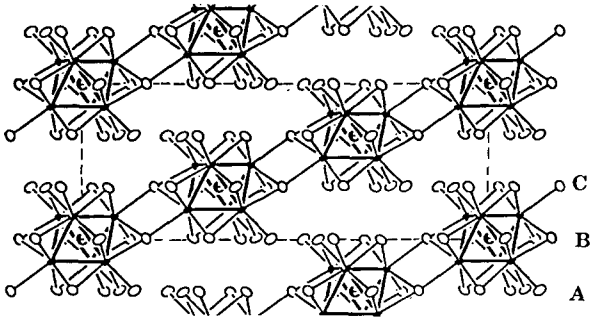

Fig. 2. [110] section of the rhombohedral $Zr_6X_{12}Be$ with the $\bar{3}$ clusters linked by six X^{i-a} bridges about the cluster waists. (The Be atom is crossed and the Zr atoms are connected by heavier lines; $\vec{c}$ is vertical.)

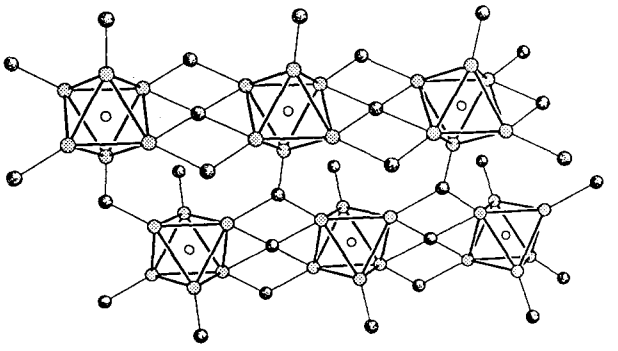

Fig. 3. Novel bridging aspects within the tetragonal structure of $Zr_6Cl_{11.5}I_{1.5}B$. The Zr_6 units are outlined, while all edge-bridging Cl, I are omitted. Note the trans-Cl^{i-i} and Cl^{a-a-a} functions (irregular shading).

$Zr_6(B)Cl_{10.4}I_{1.6}$ (the iodine mixes only on X^i sites) [10]. (The regular connectivity for this stoichiometry has recently been achieved in $Cs_4Sc_6(C)(Cl^i)_8(Cl^{i-a})_4(Cl^{a-a})_{2/2}$ [11].) Clearly the sizes of the component atoms and clusters and efficient packing may also have substantial influences on the structures chosen.

A connectivity with considerable structural variety is secured with $n = 3$, that is for $Zr_6(Z)X^i_{12}(X^{a-a})_{6/2}$. A general drive to space-filling efficiency means in practice that the detailed network disposition, even in this one series, depends on the sizes of Z, X and the number and sizes of any cations that need to be accommodated. The simple arrangement of cubic $[Zr_6(Co)Cl_{12}]Cl_{6/3}$ shown in Fig. 4 (with the 12 Cl^i atoms omitted for clarity) [12] is a stuffed derivative of the Nb_6F_{15} structure, which is in turn based on two primitive $ReO_{6/2}$ lattices in which clusters have re-

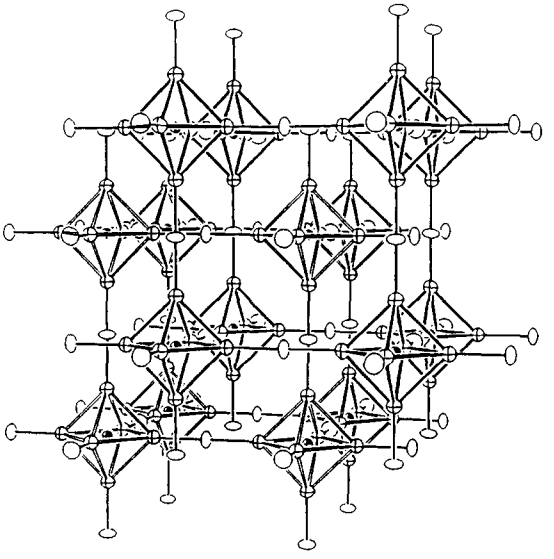

Fig. 4. A portion of the cubic structure of $[(Zr_6(Co)Cl^i_{12})]Cl^{a-a}_{6/2}$ with the inner chlorine atoms not shown. Note the two interpenetrating lattices. (Cl^{a-a} are open, Zr crossed and Co shaded ellipsoids.)

placed Re atoms. This network is proportioned just right so that, as shown, two of these can interpenetrate in a b.c.c. arrangement without any interconnections. Nothing larger than Li^+ has been accommodated in the annuli (e.g. in $Li_2Zr_6(Mn)Cl_{15}$). Five more independent ways of cluster interconnection for 6–15 compositions have been found, arrangements that cannot be interconverted without bond breakage. One cubic member, $Zr_6(N)Cl_{15}$, requires a small interstitial and, in addition, only a small amount of countercation sodium can be accommodated when the interstitial is changed to carbon. One or two larger cations can be bound in a third version, $KZr_6(C)Cl_{15}$ and $CsKZr_6(B)Cl_{15}$. (Note the electronic compensation between the number of cations and the Z electron count present in the three pairs of examples just noted.)

Two recent additions to the family occur for $Rb_5Zr_6(Be)Br_{15}$, Fig. 5 [13], and $Cs_3(ZrCl_5)Zr_6(Mn)Cl_{15}$, Fig. 6 [14]. Both illustrate another feature, that particularly the larger and less demanding cations may have to settle for relatively poor, low symmetry sites with small numbers of halide as neighbors, the dominant structure-making features evidently being associated with the cluster network. The anionic portion in the first, $Zr_6(Be)Br_{15}^{5-}$ defines a tunnel structure, and two-thirds of rubidium cations (crossed ellipsoids) within each tunnel, Fig. 5, are only three-coordinate to bromine and partially disordered. (All other Br^i have been omitted from this view for clarity.) The genesis of the part of the $Cs_3(ZrCl_5)Zr_6(Mn)Cl_{15}$ structure shown in Fig. 6 is a primitive ReO_3-like (or half of the cubic $Zr_6(Co)Cl_{15}$) network which has undergone a trigonal twist about

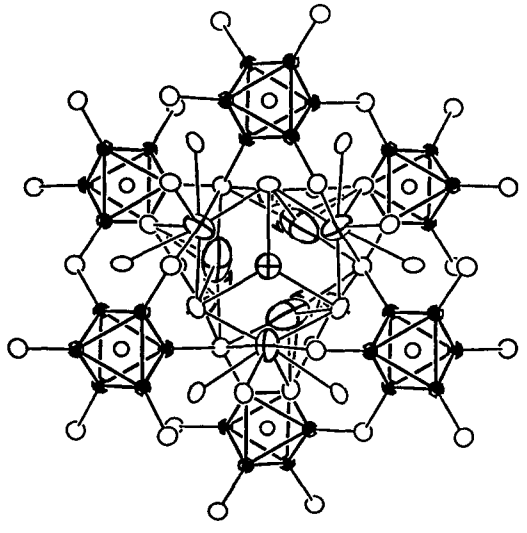

Fig. 5. A projection along the tunnels in the $Zr_6(Be)Br_{12}Br_{6/3}$ network in $Rb_5Zr_6Br_{15}Be$, the Rb ions therein (crossed), and their bromine neighbors (open).

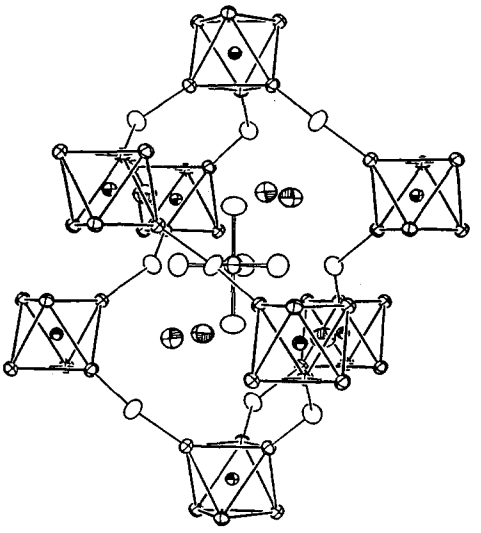

Fig. 6. One cavity in the $[(Zr_6(Mn)Cl_{12})]Cl_{6/2}^{2-}$ network (Cl^i omitted) and the $ZrCl_5^-$ and Cs^+ ions therein in $Cs_3(ZrCl_5)Zr_6(Mn)Cl_{15}$. The result is a stuffed rhombohedral perovskite.

[111] (as in RhF_3, etc.). The $ZrCl_5^{2-}(D_{3h})$ anion sits in the center of each cavity in this cluster array and does not share any halogen with it. The $(ZrCl_5)(Zr_6(Mn)Cl_{12})(Cl^{a-a})_{6/2}$ components thus correspond group-by-group to an $ABX_{6/2}$ rhombohedral perovskite. The cesium cations necessitated by the charges on the first two portions are then stuffed into fairly suitable 12-coordinate positions in this otherwise rather open structure. The fit is rather special, and the corresponding cesium boride is the only other member that has been found for this structure. However, a related bromide without the ZrX_5^- anion is achieved in $Cs_3Zr_6(C)Br_{15}$ and $Cs_{3.4}Zr_6(B)Br_{15}$ [13]. The cations now fill the central cavity somewhat, fractionally distributed over five sites that are now far from optimal in neighboring bromides (either 4 + 4 or 3 neighbors). Again, rubidium gives a different product.

The versatility provided by the several variables in these zirconium systems, both in size and in electronics, happily provides many examples (as above) of structural motifs that could never have been imagined. A new one contains A_4Br^{3+} tetrahedra in the first example of isolated halide in these relatively acidic systems. These occur in tunnels in both $(K_4Br)_2Zr_6Br_{18}B$ and $(Cs_4Br)Zr_6Br_{16}B$ [15]. As can be perceived from the stoichiometry, the first consists of isolated clusters with K_4Br^{3+} bound in tetrahedral cavities defined by Br^a; the overall arrangement is CaF_2-like. As in other systems, the 6–16 proportions of the second lead to puckered layers with $(Zr_6(Z)Cl_{12})(Cl^{a-a})_{4/2}(Cl^a)_2$ connectivities where the two exo Cl^a atoms protrude above and below the layers. In the present instance, the square layers so defined stack in an eclipsed manner so that tunnels are

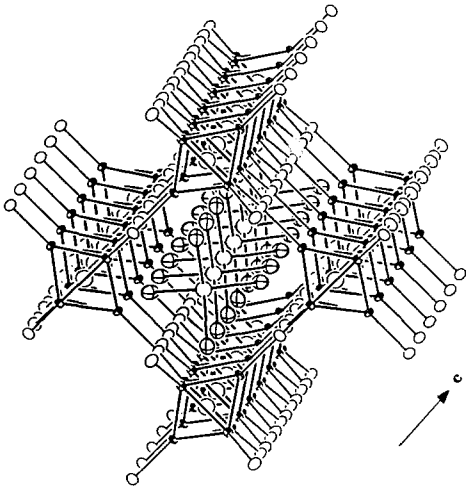

Fig. 7. A row of Cs_4Br^{3+} cations within tunnels in $(Cs_4Br)Zr_6Br_{16}B$ (Br^i omitted).

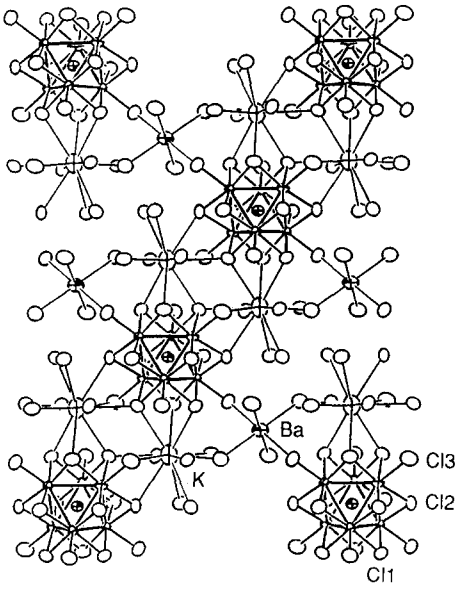

Fig. 8. [110] projection of the rhombohedral structure of $K_2BaCl_6 \cdot Zr_6Cl_{12}C$ with K and Ba sites marked.

left for columns of Cs_4Br^{3+}, Fig. 7. The cesium atoms each have nine more bromine neighbors on the tunnel walls, but these are fairly well differentiated, with the central Br shown removed by 3.36 Å, three Br^a and Br^{a-a} at 3.62–3.75 Å and six Br^i at 3.90–4.03 Å. This distribution is characteristic of the strength of A–X interactions expected, and usually observed, for halide of difference basicities and partial charges, but it is inverse to probable (small) changes in halide size.

A series of double salts in two structure types is also achieved for the chlorides [16]. A rhombohedral structure applies to $A_{1.2}MZr_6(Z)Cl_{18}$ ($= A_{1.2}MCl_6 \cdot Zr_6(Z)Cl_{12}$) with A = K–Cs. Here, all chlorine in each MCl_6 anion, M = Ca, Br, La (normal valent), are additionally bonded exo at vertices of separate $Zr_6(Z)Cl_{12}$ clusters, Z = B, C, Mn, Fe. The [110] projection of the structure of $K_2BaCl_6 \cdot Zr_6Cl_{12}C$ in Fig. 8 illustrates how well this can be described either in term of c.c.p. clusters or, more completely, as nine layers sequenced $(chh)_3$. Interstitial Z atoms at the cluster centers substitute regularly in every third chlorine layer. These are separated by pairs of chlorine layers with regular A (K) cation intervention therein, while the M (Ba) atoms lie in octahedral sites between these. M = Zr is also found as $K_2ZrCl_6 \cdot Zr_6Cl_{12}Z$ for Z = H, Be, and one iodide example is known for Cs and C [17]. An additional superstructure that involves cluster rotations but an otherwise comparable arrangement occurs with A = M in $Ba_2(BaCl_6) \cdot Zr_6Cl_{12}Be$ [18]. A small trigonal series ($Cs_2LuNb_6Cl_{18}$ type) for $A_2LaCl_6 \cdot Zr_6Cl_{12}Z$ is found when A and Z are either Cs and C, or Rb and Fe respectively. All of the above cluster members are electronically closed shell except for the hydride.

The number of centered zirconium cluster compositions achieved is well over 100. The range of Z possible in one type or another is noteworthy, as follows:

H							Be	B	C	N
								Al	*Si*	*P*
K	*Cr*	Mn	Fe	Co	Ni				*Ge*	

The italicized Z have so far been encapsulated only in iodides. The structural varieties achieved to date for zirconium iodide clusters are remarkably fewer than for the chlorides, namely only as $Zr_6I_{12}Z$, Z = H, Be, B, C, Cr, Mn and for $A_xZr_6I_{14}Z$ with A = Li–Cs and Z = B, C as well as with Z = K, Cr–Co, Al, Si, P, Ge. (There is also a mixed Si–B result obtained when an errant Pyrex glass chip in the ZrI_4 reactant was reduced [19].) Hafnium chlorides by contrast exhibit only a very modest cluster chemistry, all related to that of zirconium but apparently limited to a few carbides and borides in known structure types [20]. There is also now one example of an analogous titanium cluster, $Tl_6(C)Cl_{14}$, prepared near 500°C by a metallothermic reaction [21]. Our earlier attempts in the same system near 550°C by more traditional methods were broadly unsuccessful in producing any useful crystals, although new powder patterns were seen. It is difficult to generalize about which interstitials may be bound, or particularly, why others are not. The syntheses are carried out under equilibrium conditions, so high yields, often greater than 90%, can be expected when the right proportions are loaded. (The

phase rule indeed works.) Such a result is an excellent verification that the formula is correctly assigned and that adventitious impurities are not playing a role. It has seldom seemed worthwhile to assess what Z phases form instead when an insertion fails since the noncluster quantities are so small. However, it should be noted that for successful reactions the obvious Z alternatives, such as ZrC, ZrB_2, Pr_3Ni, $LaRu_2$, etc., together with appropriate alternate halide phases, must be less stable. Welded Ta containers are ideal, and are probably necessary for the zirconium reactions, while less expensive Nb containers appear perfectly inert for all reduced rare-earth-metal halide reactions.

3. Bonding in clusters

All theoretical treatments of nominally octahedral M_6X_{12} clusters, however modified these may be chemically, give much the same results in terms of M–M bonding descriptions, basically because of symmetry. The transformation properties of metal d (s) orbitals in clusters of or near O_h symmetry and the results when halide bonding is included are more or less fixed. (It is important, however, to include exo halides, as in an $M_6X_{12}X_6$ arrangement, as these lie trans to the M–Z bonding interactions.) The introduction of a centered interstitial hydrogen, main-group element, or transition metal, adds one (s), four (s,p) or six (d,s) more good orbitals and some additional electrons to the problem, but these introduce no new bonding states to the cluster-based levels/representations. The general ideas can be deduced from Fig. 9 [22]. On the left is a typical result, $Zr_6I_{12}I_6$ in this case, in which the most strongly bonding and principally zirconium-based levels a_{1g}, t_{1u} and t_{2g} define a 14-electron closed shell limit. (All iodine levels lie lower.) The gap to a_{2u} depends, on among other things, some relative dimensions of the cluster (below). The s and p valence levels (not shown) of a main group Z, which usually lie somewhat lower, mix with and lower the a_{1g} and t_{1u} cluster levels appreciably, with corresponding high-lying a^*_{1g} and t^*_{1u} antibonding levels being added. Thus, the usual cluster-based bonding orbitals hold 14 electrons, the foregoing a^2_{1g} and t^6_{1u} plus t^6_{2g} which is bonding solely within the cluster shell, with or without a centered main-group element. The distributions of electrons in the a_{1g} and t_{1u} levels between Z and M depends in detail on their relative valence energies, more M–M bonding being retained with higher lying Be than with C, for example [23]. Hydrogen of course lowers only the a_{1g} level (presuming it is centered).

A centered d-element interstitial alters this picture in a fairly obvious way, as shown on the right of Fig. 9.

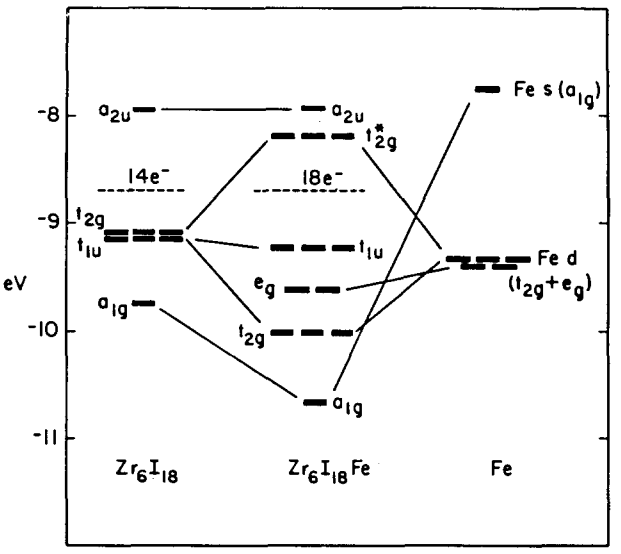

Fig. 9. Molecular orbitals for a $(Zr_6I_{12})I_6$ cluster (left) and the results when an iron interstitial (or, qualitatively, another d-element) is added. Addition of a main-group Z lowers a_{1g} (s) and t_{1u} (p) instead. The two types of centered clusters have optimal 18 and 14 cluster-based electrons respectively.

The major differences are the e^4_g valence levels on transition metal Z which have no counterpart among the lower lying, cluster-bonding orbitals and remain localized on Z. Thus, only t_{2g} (d) and a_{1g} (s) thereon mix appreciably with Zr–Zr bonding levels, while t^6_{1u} is just M–M (and M–I) bonding since p orbitals on transition metals generally lie too high to be effective. Charge presumably shifts towards Z for the later and heavier transition metals encapsulants in M_6Z. Charge estimates for Z based on Mulliken populations usually fall in the range of −0.5 to +0.5 after orbital energies have been interacted to charge consistency. It is important to note that the difference between 14 and 18 electrons for closed shells with the two types of Z, which arises because of e^4_g in the latter, means that pairs of interstitials like B and Mn, or Fe and C, are in this sense isoelectronic in their contributions to cluster bonding [24].

These guidelines have proven to be especially valid for the zirconium chlorides, where there are only a few exceptions from the 14- or 18-electron rules. This means compositions and structures can often be systematically generated or synthetically forced by the Z provided, often in concert with the amount of ACl. For instance, one series of known phases with fixed *n* is $Zr_6Cl_{15}N$, $KZr_6Cl_{15}C$, $K_2Zr_6Cl_{15}B$, $K_3Zr_6Cl_{15}Be$, and another, with fixed Z, is $RbZr_6Cl_{14}B$, $Rb_2Zr_6Cl_{15}B$, $Rb_3Zr_6Cl_{16}B$, $Rb_5Zr_6Cl_{18}B$. A majority of the exceptions to 14 electrons in chlorides are for hydrides (for which something seems to be better than nothing) in phases in which Be would give the optimal 14. Iodides are less faithful, common variants being 16 in the very stable $Zr_6I_{12}C$ and 15 in $AZr_6Cl_{14}C$ and

$Zr_6I_{12}B$. The more numerous bromide examples are intermediate in this feature and include $Cs_3Zr_6Br_{15}C$ and $Rb_5Zr_6Br_{15}Be$ [13] as 16-electron examples.

Explanations for these deviations have fairly wide applicability and are based on matrix effects, namely the alteration of distances, angles and bonding that result from closed shell contacts, often between halogen atoms. Thus there is often a dimensional conflict between optimal $M_6(Z)$ cluster size and the surrounding $12X^i$. The edge-centered cube ideally defined by X^i is usually larger than that for M_6 vertices because of close $X \cdot X$ contacts, which cause the metal vertices to lie inside the faces of the cube. This is exacerbated by large halide (I > Br > Cl), small M (Nb > Zr), and small Z (C, N, etc.). This also means that the approach of X^a to a good bonding distance from a vertex may be limited by its contacts with the four neighboring X^i. Indeed, the vertices in many $AZr_6I_{14}Z$ examples, and thence $d(Zr-I^a)$, were observed to respond inversely to the size of Z within a more or less fixed iodine array [22].

A useful measure of this matrix effect is the decrease from 180° of the trans-angle across the cube faces, $\angle X^i\text{–}Zr\text{–}X^i$ (the top vertex in Fig. 1). The correlation observed between such cluster distortions and electronic deviations appears to originate with the character of the a_{2u} LUMO (Fig. 9). This is M–M bonding but $[M(xy)\text{–}X^i(p)]$ π antibonding. Distortions — withdrawal of metal vertices from the X^i plane — reduce the π^* components and the a_{2u} level falls. Its occupancy and 16-electron species are therefore favored for large X, small M and, of course, small Z, as observed. This behavior seems widely observed [1,3,13,23] such that both centered and empty (Nb, Ta) halide clusters follow it even though the totality of bonding interactions in the two types, centered and not, differ appreciably.

Another matrix effect that is widely applicable is shown by the M–M distances in centered clusters, which are principally determined by d(M–Z) and not by M–M bonding. (The same applies in NaCl-type structures as long as the smaller component does not rattle in its neighbor's octahedron.) Cluster sizes frequently parallel those conventionally assigned to the interstitial props, although these are not always simply those inferred from Zr–Z binary phases. With transition metal Z, the Zr–Z (and R–Z) distances in the clusters are often found to be 0.1 to 0.3 Å less than in the corresponding intermetallic M_xZ compounds with similar coordination numbers for Z. Oxidation of an M_6Z portion in the intermetallic and then wrapping this with halide effectively reinforces the inward M–Z interactions. On the contrary, the smallest Z = N, H in chlorides apparently bring out a minimum zirconium cluster size that is instead defined principally by Zr–Zr interactions. Thus, the Zr–N distance in $Zr_6Cl_{15}N$ is the same as in a number of carbides, approximately 2.28 Å, not approximately 0.02 Å less as seen in each previous step Be–B–C [23]. Similarly, the distances between the cluster midpoint and Zr in $K_2ZrCl_6 \cdot Zr_6Cl_{12}H$ [25] and $Li_6Zr_6Cl_{18}H$ [26] are 2.26 Å, about 0.16 Å greater than expected for good Zr–H bonding on the basis of dimensions of other phases, ZrH_2 for instance. The implied rattling of hydrogen has been confirmed both by the room temperature relaxation characteristics of ^1H in the NMR spectrum of $Zr_6Cl_{12}H$ [27] and by an inelastic neutron scattering study of the vibration modes in $Li_6Zr_6Cl_{18}(H,D)$ at 15 K, where the latter are well described by a model of interstitial H bound in a μ_3 manner on a triangular (internal) face of the cluster [28].

4. Rare-earth metals

These elements provide a virtually unique cluster chemistry compared with that for zirconium and hafnium, doubtlessly because of the reduced number of valence electrons. Only three ternary structures contain isolated clusters, and the remainder of the reduced halides (X:R < 2:1) exhibit cluster condensation, usually through shared edges into oligomers or chains, although a variety of ternary double-metal-layered phases also exist. All cluster units contain interstitials, with many showing noteworthy encapsulation of the late and heavy transition metals, and all are hypostoichiometric (halide-poor) relative to M_6X_{12} compositions. Many of the novelties occur with iodides, while chlorides are relatively sparse in new chemistry. For instance, the Y–Cl and La–Cl systems appear to contain only a few relevant ternary phases like $Y_7Cl_{12}C$ [29]. Bromides are generally less well studied. As noted early, Y_2Cl_3, Gd_2Cl_3, Tb_2Cl_3, some analogous bromides and the odd Sc_7Cl_{10} are the only truly binary cluster phases for the group III elements, all containing chains of condensed R_6X_8-type clusters [12]. (The prospect that the Sc_7Cl_{10} composition may contain hydride cannot be excluded [30].) This section will concentrate on post-1988 results following the review by Simon et al. [2].

The variety of interstitials that have been bound is somewhat different and also larger than accomplished with zirconium, namely:

H						B	C	N
							Si	
	Mn	Fe	Co	Ni	Cu			
		Ru	Rh	Pd				
	Re	Os	Ir	Pt	Au			

It is not clear that all of the missing neighbors have been tried, Be and P for example, but the d-element

boundaries are fairly well established at least for prototypical compositions. Of course, not all R have been sampled, and there are some trends in structural stabilities with R that may extend to Z.

4.1. Clusters

The three types of discrete ternary cluster structures are the rhombohedral $R_7X_{12}Z$ and the triclinic $R_6I_{10}Z$ and $R_{12}I_{17}Z_2$. The $R_7X_{12}Z$ structure, first described for Sc_7Cl_{12} in 1978 without an identified interstitial, is derived from that of $Zr_6X_{12}Z$ (Fig. 2) by insertion of a seventh oxidized (R^{III}) metal in the antiprismatic cavity that lies midway between clusters along the $\bar{3}$ axis (z). There are some disorder problems with the seventh atom for many members with light Z [2], but heavy Z (Fe, Co) members seem well behaved [31]. The seventh R atom serves to raise the cluster bonding count from the 10 or 11 (14 or 15) that would apply in $R_6X_{12}Z$, Z = C (Fe), N (Co) to 13 or 14 (17 or 18), consistent with other systems. Attempts to substitute on that site (with Ca, etc.) have not been especially successful.

The new structure type first found for $Y_6I_{10}Ru$ [32] pertains to a good number of other components as well. The reduced halogen content is accomplished with X^{i-i} atoms that bridge edges in a pair of adjoining clusters; in fact, two pairs of X^{i-i} along with two pairs of parallel conventional X^{i-a} functions per cluster link these into infinite chains. A portion of one chain is shown in Fig. 10 for $Pr_6Br_{10}Ru$. The vertices that are not bonded in this view are actually connected by interchain X^{a-i} atoms to parallel chains. Centers of symmetry lie at Ru and at the midpoint of the above four-halogen bridge array (Br4, Br5). Systematic syntheses of $R_6I_{10}Z$ and $R_7I_{12}Z$ phases for R = Y, Pr, Gd and a large range of Z [33] and of $Pr_6Br_{10}Z$ [34] with Ru, Rh and Co show how frequently these structures occur and how widely the cluster electron counts vary. Fig. 11 shows cell volume vs. the group of Z, period by period, for $R_7I_{12}Z$ compounds of Pr, Gd, and Y (top) and for $Y_6I_{10}Z$ examples (bottom) as a demonstration of the breadth of this chemistry. The cluster electron counts are tabulated at the top of each section. In some cases as many as five consecutive 3d or four consecutive 5d interstitials can be encapsulated in a particular host. (Tc has not been tried and Ag has never been encapsulated anywhere.) Similar effects have been seen with other R, but this is the only instance where the search has been as thorough and systematic over three R members and over Z. It is worth noting again that the failure to achieve a particular target means only that alternate phases are more stable, not just that a particular combination is intrinsically poor in some respect.

Electronic reasons for the 18 ± 2 range of cluster counts seen in Fig. 4 may originate with the greater polarity of R–X (compared with Zr–X) and, in some cases, because of the properties of the late, heavy transition metal Z. First, the normal t_{1u}^6 HOMO level, which is significant only for R–R bonding (Fig. 9), may be closer to nonbonding when large Z expands the clusters ($d(Y-Y) \geq 3.7$ Å for 4d, 5d Z), and its full occupancy becomes less important. On the other side, the increasingly skewed energy diagram is predicted to

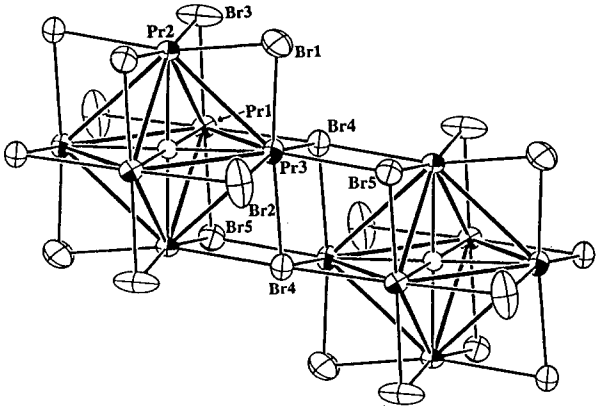

Fig. 10. One segment of the unique chains of clusters in $Pr_6Br_{10}Ru$. Note the pairs of $Br4^{i-i}$ and $Br5^{i-a}$ bridges.

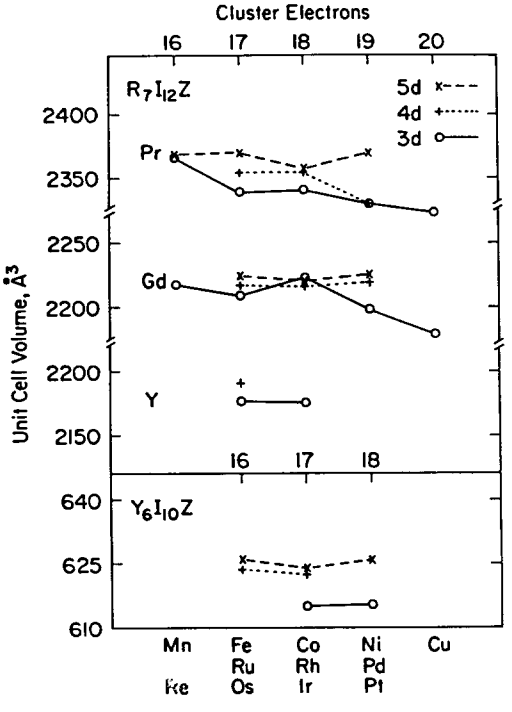

Fig. 11. Cell volume vs. group of the interstitial for $R_7I_{12}Z$ (R = Pr, Gd, Y) and $Y_6I_{10}Z$ phases. The 3d, 4d and 5d element Z are marked by ○, + and × respectively. The cluster-based electron counts are shown above each section.

place the t_{2g}^{*} R–Z antibonding level below a_{2u}, and this may be utilized for electrons above 18.

Crystal structure analyses of $Pr_6Br_{10}Ru$ with 16 and $Pr_6Br_{10}Co$ with 17 electrons per cluster together with similar data for $Y_6I_{10}Z$, Z = Ru, Os, Ir (16, 16 and 17 electrons), show some interesting distortions, as follows. An octahedron with a t_{1u}^{4} HOMO may potentially distort and both remove the degeneracy and lower the energy of the system. Contrary to common behavior in molecular systems, these octahedra compress along the quasi-four-fold axis to yield a 2-below-1 distribution rather than elongate, largely because the valence p orbitals on Z lie much too high to be influential in the R–R bonding t_{1u}. The compression is instead governed by d–d interactions in the cluster metal shell [32]. (Interestingly, this distortion route is not as obvious with the D_{3d} clusters found in $R_7I_{12}Z$ phases.) The magnitudes of these compressions, usually along the vertical R2–Z–R2 axis in Fig. 10, are described in Table 1. The 16-electron $Pr_6Br_{10}Ru$ result seems the most obvious, a 0.276 Å decrease in d(Pr–Ru) along that axis. The 0.120 Å compression for the slightly smaller 17-electron $Pr_6Br_{10}Co$ ($\bar{d}$(R–Z) decreases only 0.05 Å) presumably reflects a smaller driving force, while its occurrence along the other axis normal to the chain may simply be a size effect. The smaller R and larger X in the parent $Y_6I_{10}Ru$ example are probably responsible for a matrix effect that limits the contraction to 0.21 Å, 75% as much as for $Pr_6Br_{10}Ru$. On the contrary, the isoelectronic $Y_6I_{10}Os$ and the 17-electron $Y_6I_{10}Ir$ show, respectively, a distinctly small contraction (0.09 Å) in d(Y–Os) and a perhaps insignificant (0.035 Å) elongation of d(Y–Ir) along the chain axis. There are clearly other significant factors in the cluster distortion with these 5d elements, relativistic perhaps, that are not understood.

The third cluster structure noted above was first found for $Pr_{12}I_{17}Fe_2$ and $Pr_{12}I_{17}Re_2$ [35] and then for $La_{12}I_{17}Fe_2$ [36]. The unusually low I:R ratio with only discrete clusters in these is achieved by means of seven

Table 1
$R_6I_{10}Z$ cluster distortions [33,34][a]

Cluster electron counts	16	16	17
	$Y_6I_{10}Ru$	$Y_6I_{10}Os$	$Y_6I_{10}Ir$
$\bar{d}$(Y–Z) (Å)	2.693	2.704	2.705
Δd(Y–Z) (Å)	−0.206(5)	−0.090(2)	+0.035(1)
Y(*n*) axis	2	2	3
	$Pr_6Br_{10}Ru$		$Pr_6Br_{10}Co$
$\bar{d}$(Pr–Z) (Å)	2.787		2.739
Δd(Pr–Z) (Å)	−0.276(3)		−0.120(3)
Pr(*n*) axis	2	1	

[a] The chain axis roughly parallels R4–R3 while R2–R2 is vertical in Fig. 10. The Δd values are the odd length along the indicated axis minus the average of the other two, so a negative value is a compression.

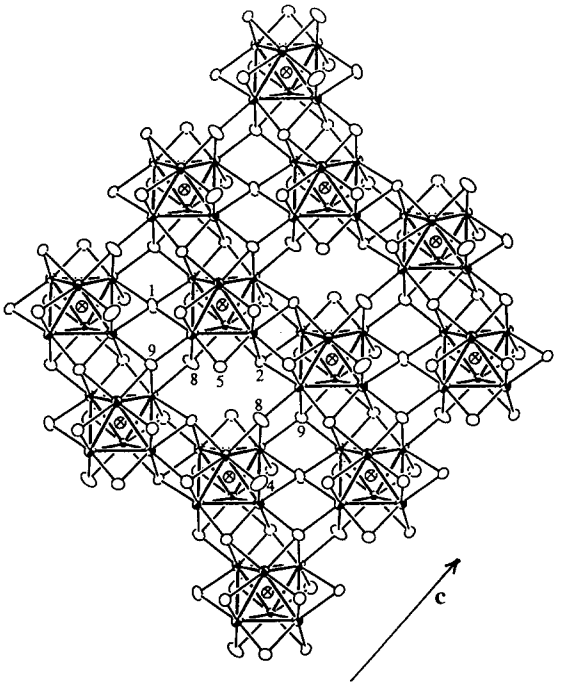

Fig. 12. One view of the triclinic structure of $Pr_{12}I_{17}Fe_2$.

I^{i-i} bridges per cluster as well as one novel I^{i-a-a} mode in a relatively complex structure. One view of this is shown in Fig. 12. The average cluster contains 17.5 electrons, but there is no evidence for different 17- and 18-electron (or other) clusters in the structure at room temperature. Further studies are under way.

4.2. Condensed clusters

A really prolific chemistry and a good variety of new phases arise in well reduced combinations of scandium, yttrium or a lanthanide element with iodine (or in some cases, bromine) and, in particular, a transition metal Z. A few examples with Z = C, Si are also known, some as chlorides [2], but the majority incorporate many of the same metals that occur within the discrete iodide clusters. Along the way are a surprising group of bromide and iodide oligomers, tetramers actually, that show well defined electronic stabilities as well.

4.2.1. Oligomers

Table 2 summarizes the four types of oligomer structure by formula and space group and also gives a further description of the component parts where appropriate, as well as the cluster-based electron counts and magnetic characteristics where known [37,38]. Fig. 13 illustrates (a) the nature of the $R_{16}Z_4$ core structure and its conceptual construction from either (b) a tetracapped truncated tetrahedron plus Z_4 or (c) a two-by-two condensation of conventional R_6Z

Table 2
A family of $R_{16}Z_4$ cluster oligomers[a]

Type	Compound	Space group	Oligomer e-count	Magnetism[b]
1	$Y_{16}I_{20}Ru_4$, $Y_{16}Br_{20}Ru_4$ $Sc_{16}Br_{20}(Re, Os)_4$	$P4_2/nmm$	60	TIP
2	$Y_{16}Br_{24}Ir_4$	$Fddd$	60	
3	$Y_{20}Br_{36}Ir_4$ $[Y_{16}Br_{24}Ir_4 \cdot 4YBr_3]$	$I4_1/a$	60	TIP
4	$Gd_{20}I_{28}Mn_4$ $[Gd_{20}I_{20}Mn_4^{4-}(Gd_4I_8^{4+})]$	$P\bar{4}3m$	60	
	$Sc_{19}Br_{28}(Fe, Ru, Os)_4$ $[Sc_{16}Br_{20}Zr^-(Sc_3Br_8^+)]$		61	C–W
	$Sc_{19+x}Br_{28}Mn_4$, $x \sim 0.6$		~59	

[a] Ref. [38] except $Y_{16}I_{20}Ru$ [37] and $Gd_{20}I_{28}Mn_4$ [39].
[b] TIP denotes temperatures independent paramagnetism, presumably van Vleck in character; C–W denotes Curie–Weiss behavior.

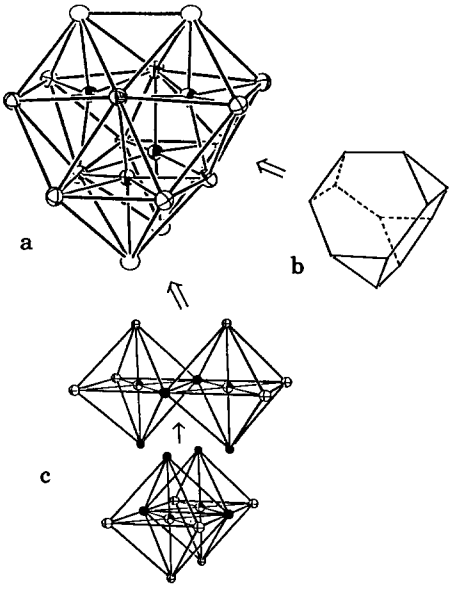

Fig. 13. The construction of (a) an $R_{16}Z_4$ cluster from (b) a truncated tetrahedron R_{12} with capping of the four hexagonal faces and insertion of a Z_4 tetrahedron or by (c) a 2 + 2 condensation of R_6Z clusters.

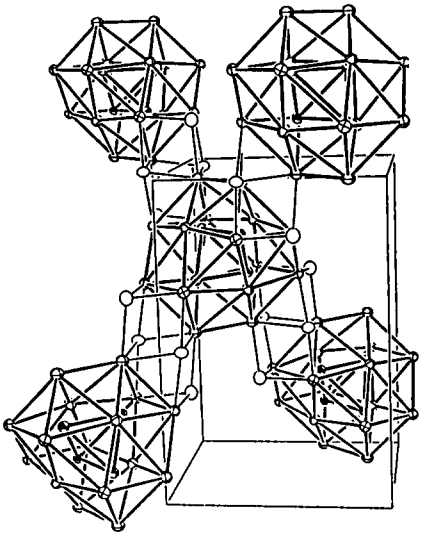

Fig. 14. One mode of intercluster iodine bridging in tetragonal $R_{16}I_{20}Z_4$. Note the vertical S_4 axis. These bridges are of the same type as in $Pr_6Br_{10}Ru$, Fig. 10.

clusters, while Fig. 14 shows a bit of how the several examples of the $R_{16}X_{20}Z_4$ stoichiometry are sheathed with halogen and interconnected by fairly normal types of halogen bridges [38]. (Note that the bridges here are of the same type as in $R_6X_{10}Z$, Fig. 10.) The four R atoms that cap hexagonal faces in Fig. 13(b) have more neighbors, 6R and 3Z, and lie outside of those faces to varying degrees (breathing). The shared edges in the imagined dimeric precursors are now defined by pairs of these face-capping R and are considerably (approximately 0.7 Å or approximately 20%) further apart than the other R–R edges. The parent octahedra in (c) have been additionally distorted by motion of the Z toward the center of the new unit, although Z–Z distances remain large in most cases (e.g. greater than 3.58 Å for Ru–Ru). A considerable matrix effect (and breathing) is evident in going from the iodide to the bromide; although the Y–Ru distances (which reflect the major bonding) remain nearly the same, the Y2–Y2 distances increase by 0.11 Å while all other Y–Y separations decrease by an average of 0.07 Å.

A second type of oligomer structure with a 16–24–4 composition (Table 2) arises when interstitial Ir is used instead of Ru; the four-electron increase therefrom is simply compensated by the addition of four more bromines to the sheath about the oligomer, this change naturally leading to fewer Y neighbors per bromine overall and corresponding changes in halide bridging functions. The pleasures derived from the discovery of new synthetic wonders were once again realized on discovery of the third type, $Y_{20}Br_{36}Ir_4$, in somewhat YBr_3-richer systems with Ir. The compound is in fact enriched by just that component, namely as $Y_{16}Br_{24}Ir_4 \cdot 4YBr_3$, a portion of which is shown in Fig. 15. Zig-zag chains of edge-sharing $Y^{III}Br_{4/2}Br_{2/2}$ octa-

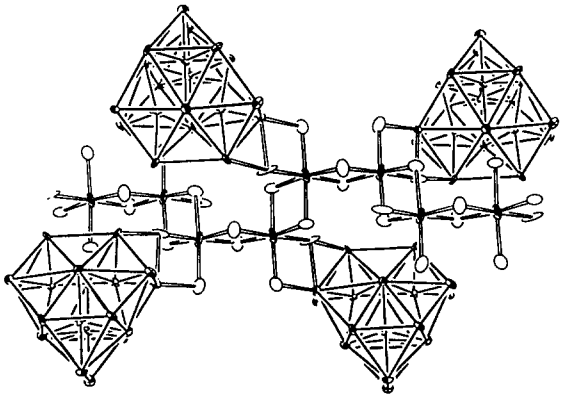

Fig. 15. The extra $YBr_{4/2}Br_{2/2}$ chain and its bridges between oligomers in $Y_{20}Br_{36}Ir_4$.

hedra now bridge between oligomers, the first four bromine functions being within the new YBr_3 chain while the last two are Br^a and Br^i to each oligomer. These are again 60-electron units. Cluster interconnections in other directions are largely as seen before and do not involve the $YBr_{6/2}$ chains. Although the imposed symmetry is different from the earlier examples, the oligomer is still very similar dimensionally. The nine distinct Br atom types exhibit five bonding modes, which will not be described further. Some fairly simple geometric relationships between oligomer placement and interconnections exist for all three structure types, at least in certain planes.

The addition of Cr, Mn, Pt or Ni interstitials to reduced yttrium bromides give none of these structure types, as might be expected for electronic reasons because of the different electron counts they would afford. Rather, the smaller scandium bromide host yields yet a fourth type for Z = Fe, Ru, Os, a cubic structure that had been seen only a little earlier with gadolinium iodide and the electron-poorer interstitial Mn. There the $Gd_{20}I_{28}Mn_4$ composition represents a similar oligomeric unit plus a second small cluster in a sphalerite-like structure [39], as shown in Fig. 16. The new tetrahedral Gd_4I_8 cluster is iodine-bridged to four oligomers, and vice versa. Both the large Gd–Gd separations in the small unit and a sparsity of bonding electrons, were this to be neutral (Gd^{II}), led to the conclusion that this must be $Gd_4I_8^{4+}$ (Gd^{III}) which functions as an electron donor and thereby again affords a 60-electron oligomer. However, EHMO calculations did not make it clear whether the unit has a closed configuration. In this case, the Mn–Mn separations are notably shorter than expected on the basis of other oligomeric structures and are apparently significant in bonding (2.82 Å, Pauling B.O. = 0.17 each); in addition, these states mix significantly with framework MO [36].

In such a structure type, the skeletal electron count

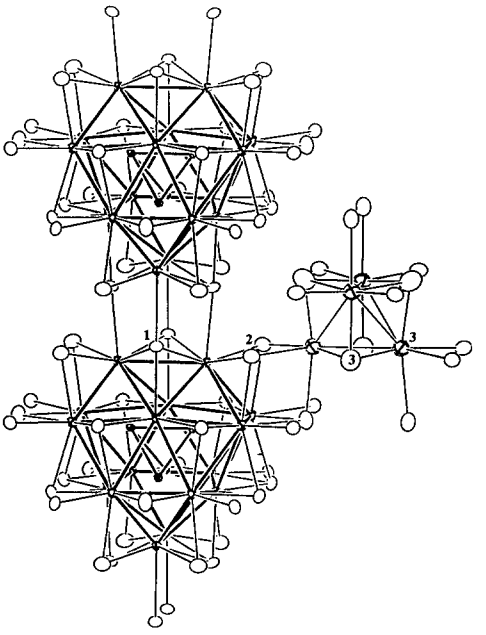

Fig. 16. The twin clusters in cubic $Gd_{20}I_{28}Mn_4$, which have been formulated as $Gd_4I_8^{4+}Gd_{16}I_{20}Mn_4^{4-}$. (Gd ellipsoids are crossed, and Mn are shaded.)

of the oligomer will necessarily change by four when the group of Z is altered by one, all other things being kept fixed. In fact, the switch from manganese to an iron group interstitial in scandium bromide analogues of the $Gd_{20}I_{20}Mn_4$ structure is largely compensated by the omission of precisely one scandium from the small cluster (disordered and probably in a quadrilled crystal) to yield a 61-electron unit (Table 2). Experimental μ_{eff} values of 2.0–2.1 (1) B.M. with Z = Fe, Ru, Os are nicely consistent with one unpaired electron per oligomer. However, the composition of the Sc–Mn member (Table 2) appears to be a less-than-ideal parallel, but d(Mn–Mn) is a short 2.79 Å and clear distortions of the oligomer generate a new a_1 LUMO within the previous gap. It should be noted that this class of compounds has been only found for the smaller R = Sc, Y and Gd and not with La or Pr. Just the converse applies for both the $R_{12}I_{17}Z_2$ cluster phases (above) and the R_4I_5Z chain compound below.

4.2.2. Chains

The novel condensed chain phases found for reduced rare-earth-metal iodides and one bromide provide further revelations about the varieties of chemistry possible. Only the four more recent, heavy-metal-centered types will be described here from among the nine ternary halide chain structure types known (excluding dicarbides) (see Ref. [2]). These newer examples generally exhibit somewhat greater breadths of suitable metal Z than do those with nonmetals (B, C), particularly for the 5d elements Os through Au as well

as Ru, Mn and Co. As a group many are also distinctive and novel examples of 1D heterometal nanowires. The examples considered will be the monoclinic single-chain R_4I_5Z, the monoclinic R_3I_3Z with double chains, the cubic polytype R_3I_3Z with a 3D network, and the square antiprismatic clusters condensed into chains, a new mode, in R_4Br_4Os. All but the last were discovered as, and have been previously described for the carbides [2].

Fig. 17 shows a portion of one chain for Pr_4I_5Ru with Pr atoms shaded, Ru crossed, and Pr–Ru bonding emphasized [40]. The octahedral units are characteristically elongated along the chain repeat relative to the shared edge, by 5.6% (0.22 Å) in this instance. The four iodines shown (open ellipsoids) each simultaneously bridge edges of two adjoining cluster units. (In addition, half of these bond exo to vertices in other chains, and vice versa.) The fifth iodine (not shown) is bonded I^{i-i} to edges of adjoining chains. Cobalt and osmium may substitute for Ru in this structure as well. As with other isolated and condensed chain phases of the rare-earth elements, Pr_4I_5Ru shows neither any magnetic effects from the interstitial nor significant coupling between the $4f^2$ cores of the framework Pr, giving rather Curie–Weiss behavior down to 6 K (μ_{eff} = 3.5 B.M. per Pr vs. 3.58 B.M. classically, θ = −20.8 K). The lanthanum analogue exhibits only a small temperature-independent paramagnetism appropriate to a Pauli-paramagnetism of conduction electrons. This property is consistent with the metallic behavior predicted by 1D extended Hückel band calculations on the iodide-sheathed chain in Pr_4I_5Ru. The composite DOS results are shown in Fig. 18 with individual contributions from I (open), Pr (hatched), and Ru (black area) projected out [40]. (The use of charge consistent orbital energies is also appropriate in these instances so as to reflect the unusual environment of particularly the Ru.) The valence band centered around − 11.4 eV contains mainly iodine p plus metal components consistent with Pr–I bonding. The broad conduction band contains only metal states, with Ru making significant contributions mostly near and below E_F. This presents an interesting and sensible

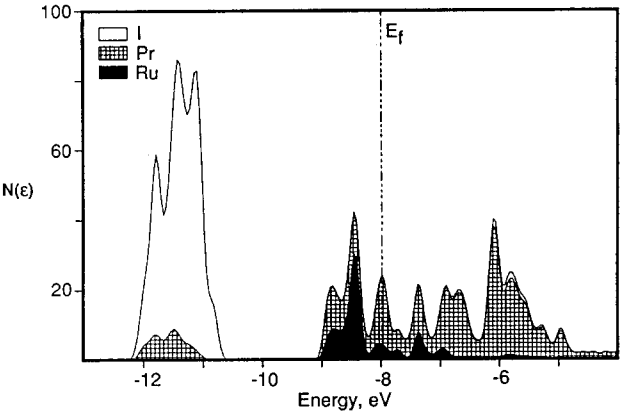

Fig. 18. DOS results from an extended Hückel calculation on Pr_4I_5Ru. The contributions from Pr, Ru and I throughout are shown as crossed, black and white areas respectively.

contrast with the band distributions in the isostructural Y_4I_5C where the Pr–C valence band falls 3–4 eV below E_F and the conduction band is substantially all Y-based [41]. The apical Pr–Ru separation in Pr_4I_5Ru is 0.33 Å less than those along the chain, representing more effective d orbital bonding in that direction than found with p orbitals on a main-group Z like Si.

End views of the double-chains in two examples of the monoclinic R_3I_3Ru (R = La, Pr, Gd, Y, Er) and R_3I_3Ir (R = Gd, Y) structure shown in Fig. 19 reveal a surprising effect. The left view, slightly off [010], is that of Pr_3I_3Ru and affords a clear perception of a pair of chains (as seen individually in Pr_4I_5Ru) displaced from each other by $b/2$ and further condensed through the sharing of side edges (a mode already known in $Sc_7Cl_{12}C_2$ and Y_6I_7C). (The reduction in iodine content from R_4I_5Z comes from a new five-coordinate interchain bridging function.) The projection changes considerably on switching to that of Y_3I_3Ir on the right side of Fig. 19. There pairs of octahedra that defined the double chains before have now virtually disappeared as the chains have more-or-less moved into each other. The apex–Z–apex angular distortion of the individual cluster components from

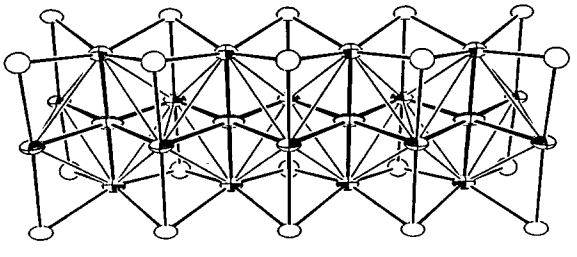

Fig. 17. A side view of the condensed chain in Pr_4I_5Ru. Note the trans-edge-sharing $Pr_{4/2}Pr_2(Ru)$ clusters (Pr–Ru emphasized) and the iodines that each bridge two cluster edges (light lines).

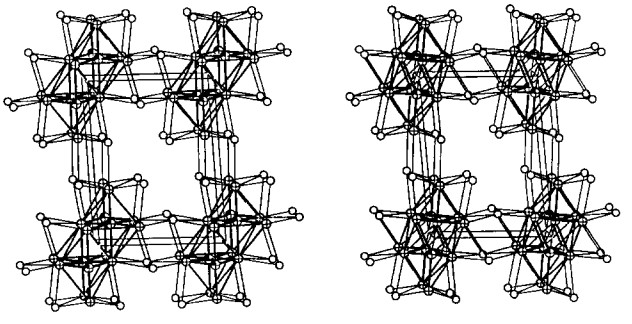

Fig. 19. Projections down the condensed double chains in monoclinic Pr_3I_3Ru (left) and Y_3I_3Ir (right). Note the absence in the right view of the cluster octahedra that are apparent on the left.

about 180° to about 154° resembles more that seen in the formation of oligomers (Fig. 13). The distortion is not well understood but shorter Z–Z and R–R distances are obtained [42]. The R_3I_3Ru members for R = Y, Gd, Er appear to exhibit intermediate degrees of distortion. An even greater distortion than that in Y_3I_3Ir appears with an electron-poorer Z in the isostructural Gd_3I_3Mn, where d(Mn–Mn) is 2.66 Å (×2) [39]. Electronically, La_3I_3Ru exhibits a small and nearly temperature-independent paramagnetism. Band calculations place the Pr–Ru band in the fairly undistorted Pr_3I_3Ru about 0.6 eV below E_F and suggest a narrow gap at E_F. The observed distortions may well be electronically driven.

Cubic R_3I_3Z phases for R = La, Pr with a sizeable range of Z, Os–Au (not established for all combinations), and Pr_3Br_3Z for Z = Os, Co, Rh, Ir, Pt are all isostructural with Ca_3PI_3 (and Gd_3I_3C [2]) and contain 3D networks of intersecting 4_1 chains formed through sharing of three non-adjacent edges of each $R_6(Z)$ cluster. All halogen is now X^{i-i-i} to three adjoining clusters. This is another case in which binding of 5d elements appears to be favored. The lanthanum examples appear to be poor metals judging from susceptibility and qualitative resistivity measurements [43]. There are of course no general rules regarding the electronic stability of any of these chain compounds. Those that accommodate a range of electronically different Z probably have an open band and are generally metallic, as with these cubic R_3I_3Z phases. However, La_4I_5Ru seems to be metallic as well, so the limited Z range there is apt to more thermodynamically based. The undistorted monoclinic Pr_3I_3Ru (above) may have a narrow gap at E_F, but the distortions found with Ir cloud any simple picture.

Although the foregoing certainly qualify as unusual when judged from the status of the field 10–15 years ago, one is never prepared for the unprecedented that were recently revealed in the last two compound types to be described, R_4Br_4Os (R = Y, Er) [44] and LaI [6]. The two bromides are the only well characterized halide examples of chains generated from confacial, centered square-antiprismatic clusters, although some relatively intractable and apparently related possibilities have been seen in iodides with small R [34], and other heavier R prospects have not been explored well. Atom sizes are again evidently quite important to gain this structure with its interbridged chains and robust crystals. The character of the bromide structure is shown in projection in Fig. 20. The bromine atoms tilt off the planes of the shared faces so that they cap half of the eight triangular faces about the waist of each antiprism; these systematic displacements alternate so as to allow the vertices thereby exposed to bond exo to bromine on other chains. The small chain distortions accompanying these displacements appear

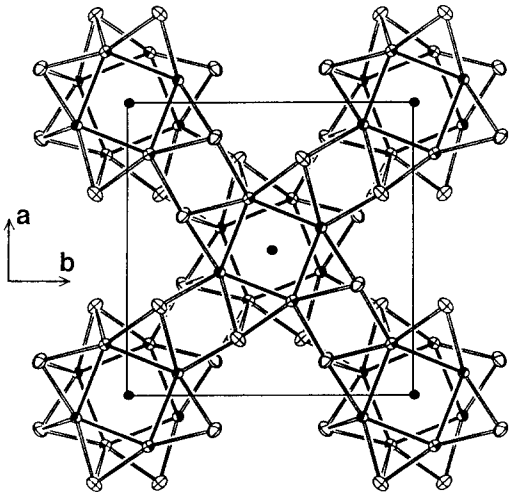

Fig. 20. Projection of the tetragonal structure of Y_4Br_4Os down the chain axis. The confacial $Y_{8/2}$ antiprisms are highlighted. All bromine atoms cap triangular faces on the antiprisms and also bond to metal vertices in adjoining chains.

to be well compensated by the fourth interchain bonding interaction by bromine, the distance in fact being only slightly larger than those within the face-capping mode. In contrast, face capping of centered octahedral clusters is probably precluded by short Z···X separations that would be generated across that face. Kindred antiprismatic examples such as Ta_4Te_4Si [45] have distinctly different chain proportions, and the chains are held together only by packing and dispersion forces, not bridging atoms. Amusingly, Ta_4Te_4Si and Y_4Br_4Os are isoelectronic (recall the Fe–C comparison made earlier where e_g^4 in the former is nonbonding). However, size proportions are quite different, the relatively small Si yielding much more compressed antiprisms so that Si–Si interactions down the chain become significant. Ahn et al. [46] have recently provided considerably more characterization of these bromides and several of the tellurides. The bromides are small-gap semiconductors, while the tellurides centered by Cr, Fe or Co are metallic over large temperature ranges. These properties are also consistent with the results of their extended Hückel band calculations.

Finally, the significance of the discovery of a truly binary LaI in a NiAs-type structure is particularly high in light of several early reports of RX phases in ZrCl or ZrBr (double-metal-layered) arrangements. The latter have now all been correctly identified as RXH_n examples, approximately $0.6 < n < 1$, (e.g. Ref. [47]), and a substantial interstitial chemistry of R–X–Z phases has subsequently been developed in the same or generally related structures [2]. The discovery of LaI was clearly delayed and complicated by a very slow rate of formation, probably because of both the blockage of La surfaces afforded by the metallic LaI_2

and the relatively low decomposition temperature of LaI, about 800°C. Its hexagonal NiAs structure exhibits a record high c/a ratio of 2.47, this flexibility allowing strong La–La bonding to be achieved in the basal plane even in the presence of a relatively large anion. (In other words, the LaI_6 trigonal antiprisms are severely elongated but with retention of reasonable La–I distances, and the La–La separations along c that are so familiar in this structure type are 24% longer.) An important aspect that appears to distinguish this structure from the ternary hydrides is that the NiAs lattice does not contain any reasonable sites for interstitial hydrogen and, of course, the phase can be regularly prepared in high yield without hydrogen. The LaI is Pauli-paramagnetic and a strongly anisotropic conductivity is expected according to band calculations. The LaI example is so far a singularity, but other examples are being pursued.

There is doubtlessly much left to be found, just for the looking.

Acknowledgements

A great deal of the credit for the discoveries accomplished in Ames and described above belongs to the 15 or so graduate and postdoctoral students whose names appear in the references. This research has been supported by the National Science Foundation — Solid State Chemistry — via Grant DMR-9207361 (and earlier grants) and has been carried out in the Ames Laboratory, DOE.

References

[1] R.P. Ziebarth and J.D. Corbett, *Acc. Chem. Res., 22* (1989) 256.
[2] A. Simon, Hj. Mattausch, G.J. Miller, W. Bauhofer and R.K. Kremer, in K.A. Gschneidner and L.üEyring (eds.), *Handbook on the Physics and Chemistry of Rare Earths*, Kluwer Academic Publishers, 1992, Vol. 15, p. 191.
[3] J.D. Corbett, in E. Parthé (ed.), *Modern Perspectives in Inorganic Crystal Chemistry*, Kluwer Academic Publishers, 1992, p. 27.
[4] F. Böttcher, A. Simon, R.K. Kremer, H. Buchkremer-Hermanns and J.K. Cockcroft, *Z. Anorg. Allg. Chem., 598/599* (1991) 25.
[5] F.A. Cotton and W.A. Wojtczak, *Inorg. Chim. Acta, 223* (1994) 93.
[6] J.D. Martin and J.D. Corbett, *Angew. Chem. Int. Ed. Engl., 34* (1995) 233.
[7] H. Schäfer and H.-G. Schnering, *Angew. Chem., 76* (1964) 833.
[8] A.F. Wells, *Structural Inorganic Chemistry*, Clarendon Press, Oxford, 1984, 5th edn., Chapter 9.
[9] H.M. Artelt, F. Schleid and G. Meyer, *Z. Anorg. Allg. Chem., 618* (1992) 18.
[10] M. Köckerling, R.-Y. Qi and J.D. Corbett, *Inorg. Chem.*, submitted.
[11] H.M. Artelt, F. Schleid and G. Meyer, *Z. Anorg. Allg. Chem., 620* (1994) 1521.
[12] J. Zhang and J.D. Corbett, *Inorg. Chem., 30* (1991) 431.
[13] R.-Y. Qi and J.D. Corbett, *Inorg. Chem., 34* (1995) 1657.
[14] J. Zhang and J.D. Corbett *Inorg. Chem., 34* (1995) 1652.
[15] R.-Y Qi and J.D. Corbett, in preparation.
[16] J. Zhang and J.D. Corbett *Inorg. Chem., 32* (1993) 1566.
[17] M.W. Payne and J.D. Corbett, *J. Solid State Chem., 102* (1993) 553.
[18] J. Zhang and J.D. Corbett, *Z. Anorg. Allg. Chem., 598/599* (1991) 363.
[19] G. Rosenthal and J.D. Corbett, *Inorg. Chem., 27* (1988) 53.
[20] R.-Y. Qi and J.D. Corbett, *Inorg. Chem., 33* (1994) 5727.
[21] D.J. Hinz and G. Meyer, *J. Chem. Soc., Chem. Commun.*, (1994) 125.
[22] T. Hughbanks, G. Rosenthal and J.D. Corbett, *J. Am. Chem. Soc., 110* (1988) 1511.
[23] R.P. Ziebarth and J.D. Corbett, *J. Am. Chem. Soc., 111* (1989) 3272.
[24] T. Hughbanks, *Prog. Solid State Chem., 19* (1989) 329.
[25] H. Imoto, J.D. Corbett and A. Cisar, *Inorg. Chem., 20* (1981) 145.
[26] J. Zhang, R.P. Ziebarth and J.D. Corbett, *Inorg. Chem., 31* (1992) 614.
[27] P.J. Chu, R.P. Ziebarth, J.D. Corbett and B.C. Gerstein, *J. Am. Chem. Soc., 110* (1988) 5324.
[28] J.D. Corbett, J. Eckert, U.A. Jayasooriya, G.J. Kearley, R.P. White and J. Zhang, *J. Phys. Chem., 97* (1993) 8384.
[29] H.-J. Meyer and J.D. Corbett, unpublished results.
[30] F.J. DiSalvo, J.V. Waszczak, W.M. Walsh, Jr., L.W. Rupp, Jr. and J.D. Corbett, *Inorg. Chem., 24* (1985) 4624.
[31] T. Hughbanks and J.D. Corbett, *Inorg. Chem., 27* (1988) 2022.
[32] T. Hughbanks and J.D. Corbett, *Inorg. Chem., 28* (1989) 631.
[33] M.W. Payne and J.D. Corbett, *Inorg. Chem., 29* (1990) 2246.
[34] R. Llusar and J.D. Corbett, *Inorg. Chem., 33* (1994) 849.
[35] Y. Park and J.D. Corbett, *Inorg. Chem., 33* (1994) 1705.
[36] J.D. Martin and J.D. Corbett, in preparation.
[37] M.W. Payne, M. Ebihara and J.D. Corbett, *Angew. Chem. Int. Ed. Engl., 30* (1991) 856.
[38] S.J. Steinwand and J.D. Corbett, in preparation.
[39] M. Ebihara, J.D. Martin and J.D. Corbett, *Inorg. Chem., 33* (1994) 2079.
[40] M.W. Payne, P.K. Dorhout and J.D. Corbett, *Inorg. Chem., 30* (1991) 1467.
[41] S.M. Kauzlarich, T. Hughbanks, J.D. Corbett, P. Klavins and R.N. Shelton, *Inorg. Chem., 27* (1988) 1791.
[42] M.W. Payne, P.K. Dorhout, S.-J. Kim, T.R. Hughbanks and J.D. Corbett, *Inorg. Chem., 31* (1992) 1389.
[43] P.K. Dorhout, M.W. Payne and J.D. Corbett, *Inorg. Chem., 30* (1991) 4960.
[44] P.K. Dorhout and J.D. Corbett, *J. Am. Chem. Soc., 114* (1992) 1697.
[45] M.E. Badding and F.J. DiSalvo, *Inorg. Chem., 29* (1989) 3952.
[46] K. Ahn, T. Hughbanks, K.D.D. Rathnayaka and D.G. Naugle, *Chem. Mater., 6* (1994) 418.
[47] Hj. Mattausch, R. Eger, J.D. Corbett and A. Simon, *Z. Anorg. Allg. Chem., 616* (1992) 157.